JOM, Vol. 74, No. 2, 2022
https://doi.org/10.1007/s11837-021-05057-3

Separation of Mn and Fe from a Manganiferous Iron Ore Using Horse Dung as Reductant: A Zero Waste Approach

SONER TOP,[1] MAHMUT ALTINER ,[2,3] and SAIT KURSUNOGLU[1]

1.—Department of Nanotechnology Engineering, Abdullah Gul University, 38100 Kayseri, Turkey. 2.—Department of Mining Engineering, Division of Mineral Processing, Cukurova University, 01330 Adana, Turkey. 3.—e-mail: maltiner@cu.edu.tr

The separation of manganese and iron from a manganiferous iron ore using horse dung (biomass) as reductant was investigated in a sulfuric acid solution, and 99.80% Mn and 17.76% Fe were extracted into the solution under these leaching conditions: 1 M sulphuric acid concentration, 120 g/L biomass, 1/10 solid to liquid ratio, 300 rev/min stirring speed, 90°C leaching temperature, and 3 h leaching time. In the first precipitation step, the iron and aluminum were first rejected from the solution at pH 5.04. Thereafter, 98.58% Mn was precipitated at pH 10 in the second step. The precipitate was identified as a pyrochroite mineral. After the leaching, the residue was subjected to a carbothermal reduction process conducted at 700°C for 10 min in the presence of no extra reductant. The residue was converted to magnetite mineral, which can be easily recovered by magnetic separation. Based on the experimental results, a flowsheet has been proposed.

INTRODUCTION

Manganese is a strategic element for the application of industrial processes. More than 80% of manganese is used in the iron and steel production industries. It is also utilized for the production of batteries, glass, fertilizers, food additives, pharmaceuticals, chemicals, and fireworks.[1] In steel production, manganese mainly provides the removal of impurities such as phosphorus, sulfur, and silica. Furthermore, it increases the workability properties and strength of steel.[2]

Manganese ores are divided by Chinese industrial authorities into two main categories according to Mn/Fe ratios. These are commercial value manganese ores with an Mn/Fe ratio of 5 and ferruginous manganese ores with an Mn/Fe ratio of less than 3.[3] The Indian mining bureau has also classified manganese ores into three main categories: (1) manganiferous iron ores (10% < Mn < 25% and Fe < 48%), (2) ferrous manganese ores (25% < Mn < 35% and 13% < Fe < 23%), and (3) manganese ores (> 35% Mn and without Fe).[4]

(Received August 14, 2021; accepted November 17, 2021; published online January 13, 2022)

Manganiferous iron ores were used in the late 19th and early 20th centuries for the production of spiegeleisen which was identified as a ferromanganese alloy containing 15% manganese, 80% iron, and smaller amounts of carbon and silica. The most popular production method of the steel production processes of this period was the Bessemer process. Manganiferous iron ores were either mixed with iron ores or fed directly into the furnace for steel production.[5] As a result of the technological developments in steel production processes and furnaces at the end of the twentieth century, the use of ferromanganese alloys containing 70–80% manganese became more common in the industry, and the importance of high-grade manganese and Fe-Mn ores increased dramatically. However, the increasing demand in recent years and the depletion of reserves of high-grade manganese ores have caused the researchers to focus on the extraction of manganese from low-grade manganese ores, especially manganiferous iron ores.

Due to the deoxidation and desulfurization abilities of Mn oxides, Mn grades are required to be below 1.5% for direct charge iron ores and below 5% for sintered ores.[6] The reason why manganese grades are desired at these rates is that they have a negative effect on the reduction of iron ores in the

furnace. High Mn grades in iron ores cause a heterogeneous reduction in the furnace and mixing of valuable iron contents into the slag. In addition, the Mn/Fe ratio should be higher than 5 for ferromanganese production in manganese ores.[7]

Iron can be easily separated from gangue minerals by using the density, magnetic susceptibility, and surface properties. The same separation techniques can also be used for manganese.[8–12] However, if iron and manganese are present in the same ore, these conventional mineral processing techniques are not efficient to obtain two main streams of the product.[3,13,14] This is due to the chemically similar properties and close relationship in the periodic table.[15–17] For this reason, MnO_2 and Fe_2O_3 are converted into non-magnetic MnO and ferromagnetic Fe_3O_4 by a carbothermal reduction method using coal and carbon monoxide,[18,19] and then the separation efficiency is increased a little bit more.[3,20] Pyrometallurgical processes are also not economical as they require high temperatures. In addition, after roasting with sulfur dioxide, only manganese ores can be converted into manganese sulfate compounds and separated by water leaching.[21]

Manganese, which is found in various stable forms, Mn(II), Mn(III), and Mn(IV) in nature, can be transformed into more stable compounds with changes in Eh and pH values. To reduce the high-valance Mn(III) and Mn(IV) to Mn(II) with lower Eh values, reductive leaching has been carried out in an acidic solution. The reduction reaction of MnO_2 in an acidic medium is:

$$MnO_2 + 4H^+ + 2e^- \rightleftharpoons Mn^{2+} + 2H_2O \qquad (1)$$

Recently, manganese has been extracted the manganese ores and manganese–iron ores by reductive leaching using carbohydrates,[22–25] pyrite,[26] methanol,[27] SO_2,[28] oxalic acid,[29] biomasses,[30–34] hydrogen peroxide,[35,36] formic acid,[37] CaS,[38] tannic acid,[39] and ascorbic acid[40] as reductant. The use of biomass as the ore reductant has superior advantages, such as price, availability, and lower pyrolysis temperature, compared with traditional coal reductant.[41] These advantages decrease production costs and energy consumption.

However, the reductive leaching of manganese from the manganiferous iron ores by using animal droppings as a reducing agent has not previously been reported in the literature. In this study, the reductive leaching of manganese from the manganiferous iron ore using horse dung (biomass) as a reducing agent in a sulfuric acid solution has been investigated. After the reductive leaching experiments, insoluble biomass in the leach residue was used as reductant to convert undissolved high iron content to magnetite mineral, which can be easily separated from gangues by magnetic separation. In addition, the precipitation of manganese from the pregnant reductive leach solution was performed.

MATERIALS AND METHOD

Material

The ore sample was taken from Sonmez Cementin Ceyhan-Adana, Turkey. The sample was first crushed by a laboratory jaw crusher (Baz-BZ923B) and then subjected to a laboratory ball mill (Rantek). The particle size distribution of the ground sample was determined by a Malvern Mastersizer 2000. To determine the chemical composition of the sample, a certain mass of the sample was completely dissolved in a hot aqua regia, and then the element contents were analyzed by an atomic absorption spectrophotometer (AAS; Perkin Elmer PinAcle 900 F) at Abdullah Gul University, Nanotechnology Department (AGU) and an AAS (Perkin Elmer PineAcle 900 H) at Cukurova University Mining Engineering Department (CU). The loss on ignition (LOI) value of the sample was calculated from the weight loss of the sample kept in a muffle furnace at 1000°C for 1 h. The total sulfur content was determined using an Eltra CS 580 instrument. Phosphor content was analyzed by a Nanocolor 100D spectrophotometer at CU's Environmental Engineering Department. The chemical composition was also confirmed by x-ray fluorescence (XRF; Minipal 4 Panalytical). X-ray diffractometer (XRD) analysis was performed by a Bruker D8 Discover instrument equipped with Lynxeye detector to determine the mineralogical composition of the sample at AGU's Central laboratory. The XRD measurements were taken for 15 min in the range of 10–90°, and step size was 0.02°. The mineral identification was evaluated using Diffrac Suite Eva software, which has an up-to-date PDF 2 database. The mineral morphology was also investigated by scanning electron microscopy (Zeiss Gemini SEM 300) at AGU's Central laboratory.

The biomass was first dried in an oven at 105°C until it reached a constant weight and then fed into a laboratory ball mill. After 30 min grinding, the biomass was analyzed by Fourier transform infrared spectroscopy (FT-IR; Thermo Scientific Nicolet 6700). The calorific analysis of the biomass was performed by an IKA C 200 calorimeter. To determine organic acids in the biomass, the waste biomass was leached in the absence of manganiferrous iron ore under the following conditions: 1 M sulfuric acid concentration, 120 g/L biomass, 90°C leaching temperature, and 3 h leaching time. After the leaching was completed, the leach liquor was analyzed by high-performance liquid chromatography (HPLC; Shimadzu Nexera X2) at CU's Central laboratory. The analysis of the sample was carried out in an ICSep ICE-Coregel 87H (30 cm × 7.8 mm × 9 μm; Transgenomic, USA) column. The separated components were monitored with a refractive index detector. The optimum chromatographic separation was achieved at 4 mM H_2SO_4 mobile phase, 0.4 mL/min flow rate, and 55°C column temperature.

Method

The reductive leaching tests were carried out in a 250-mL flat-bottomed two-necked reactor equipped with a glass spiral-type reflux condenser. A temperature-controlled magnetic stirrer (MTOPS MS300HS) was used for mixing. The temperature was controlled with a glass thermometer fixed on the reactor. Analytical grade chemicals (Merck or Sigma Aldrich) and deionized water were used for chemical preparation. The leaching parameters were kept constant at a particle size of − 100 μm, a solid to liquid ratio of 1/10 (w/v), and a sulfuric acid concentration of 1 M according to the preliminary tests. It has been reported in the literature that the stirring speed has no significant effect on manganese dissolution above 250 rpm.[38,42] Therefore, the stirring speed of 300 rpm was also selected as a fixed parameter in the leaching tests. After the leaching experiment finished, the slurry was filtered using Whatman 1 filter paper and the residue was washed with deionized water. The leach solutions were measured and analyzed by AAS to determine the elemental compositions. The extraction percentages of the metals were calculated based on Eq. 2. The leach residue was also analyzed by XRF and XRD.

$$Extraction(\%) = \frac{C_t \times V_F}{W_0 \times H_0} \times 100 \qquad (2)$$

where C_t is the metal concentration in the leachate (mg/L), V_F the volume of the analysed leachate (L), H_0 the metal concentration in the feeding (mg/kg), and W_0 the weight of the feeding sample (kg).

The carbothermal reduction experiments were carried out on the reductive leach residue where the highest Mn leaching conditions were determined. The experiments was conducted at 600–900°C in a muffle furnace. The reductive leach residue was weighed and transferred in a crucible. When the muffle furnace reached a desired temperature, the crucible was put into the muffle furnace. After the reduction period was completed, the crucible was taken from the furnace and the residue in it was poured into water (water-quenching) without delay to prevent re-oxidation and contact with air. During the carbothermal reduction tests, undissolved biomass in the residue provided carbon requirements resulting in the transformation of leach residue into magnetite mineral. No extra reductant was used. The XRD patterns were also plotted to determine the phase conversion.

In the precipitation experiments, a certain volume of pregnant leach solution (PLS) was poured into a beaker and placed on a heating mantle equipped with a magnetic stirrer. The mixing speed was kept constant at 350 rpm. The pH of the solution was monitored with a Hach HQ40d pH meter. When the solution reached a certain temperature, sodium hydroxide (5 M) was slowly delivered by a syringe until the targeted pH value. When the desired pH was achieved, the solution was stirred for 30 min. When the time was completed, the slurry was filtered through Whatman 1 filter paper using vacuum filtration. The contents of the test filtrate and washing filtrate were measured and analyzed by AAS. The precipitation percentages of the metals were calculated according to Eq. 3:

$$Precipitation_{(M)}(\%) = \frac{[C_{Initial}.V_{Initial} - (C_{Filtrate}.V_{Filtrate} + C_{Wash}.V_{Wash})]}{C_{Initial}.V_{Initial}} \times 100 \qquad (3)$$

where M is metal, C_{Initial}, and C_{Filtrate}, and C_{Wash} are the test solution, filtrate, and wash liquor concentrations (mg/L) of the individual element and V_{Initial}, V_{Filtrate}, and V_{Wash} are the test solution, filtrate, and wash liquor volume (L), respectively.

All the tests were duplicated to assess the reproducibility of the test results. Standard deviation values in the leaching and the precipitation tests ranged from 0.01 to 3.17.

RESULTS AND DISCUSSION

The particle size analysis revealed that less than 80% of the sample was determined to be ~ 50 μm, which has been used for the further reductive leaching experiments (see online supplementary Fig. S-1). The chemical composition of the sample is given in Table I. The chemical analysis demonstrated that the sample can be classified as a manganiferous iron ore. The XRD pattern of the sample is shown in Fig. 1. The crystal phase of the sample consists of 16.3% hematite (PDF Card No: 33-0664), 16.1% goethite (PDF Card No: 81-0464), 14.8% manganite (PDF Card No: 08-0099), 12.7% maghemite (PDF Card No: 39-1346), 12.5% grossular (PDF Card No: 03-0801), 9.2% quartz (PDF Card No: 46- 1045), 8.3% calcite (PDF Card No: 05-0586), 7.8% ramsdellite (PDF Card No: 42-1316), and 2.2% calcite-magnesian (PDF Card No: 86-2336) minerals.

When the elemental mapping images are examined, it can be seen that the manganese and iron minerals (hematite, goethite, manganite, and ramsdellite) exist together, while the aluminum, silicone, and calcium minerals are hosted in the same places (see supplementary Fig. S-2). Due to the interlocking structure of manganese and iron contents, a physical separation method is not considered as a favourable choice.

FT-IR analysis of the biomass shown in Fig. S-3 revealed that the wavenumber region between 950 cm^{-1} and 1200 cm^{-1} contains functional groups mainly from carbohydrate.[43] The main absorbance determined at 1036 cm^{-1} indicates the C–O bonds in the material. The peak at 1415 cm^{-1} represents a methyl asymmetric C–H and O–H bindings and –CH_2.[44–46] The peaks between 1632 cm^{-1} and 1657 cm^{-1} are proteins and peptides.[47,48] The peaks at

Table 1. Chemical analysis of the sample

Content	Fe	Mn	Al	Ca	Mg	P	S	LOI[a]
%	25.04	15.03	1.54	3.29	0.94	0.18	0.11	10.89

[a]Loss on ignition.

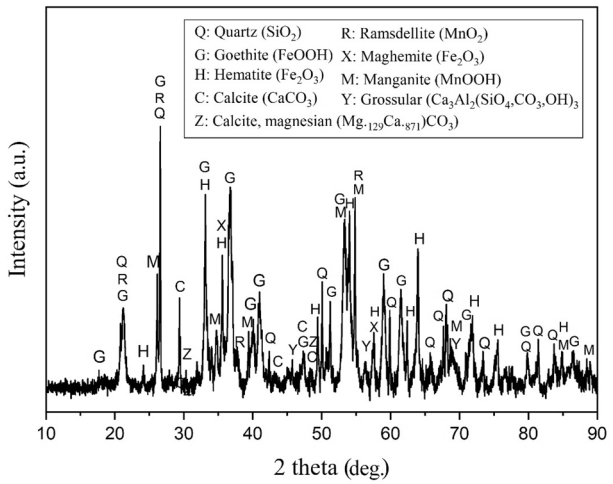

Fig. 1. XRD pattern of the sample.

2850 and 2924 cm^{-1} are characterized by fat and lipids. For the lower frequencies, the peak at 3260 cm^{-1} is due to N–H stretching of proteins and O–H stretching of water and carbohydrates, while the peak at 2928 cm^{-1} is due to CH_2 antisymmetric stretch of methyl groups mainly from lipids.[43] The FT-IR analysis is consistent with the findings of characteristics of sewage sludge wastes.[49,50] The calorific value of the biomass was found to be 3674 kcal/kg.

Leaching Experiments Without Reductant

The leaching experiments were performed at four different temperatures and varying H_2SO_4 concentrations (Fig. 2). It was observed that temperature has a crucial effect on the extraction of iron. At 90°C, the iron extraction is around 80% using 4 M and 5 M H_2SO_4 concentrations. It was also seen that the aluminum extraction increases with increasing leaching temperature. The manganese extraction slightly increased with increasing leaching temperatures, but the extraction values did not exceed 30% even at 5 M H_2SO_4 concentration and 90°C temperature. There are no regular increases in calcium extraction values. This stems from the precipitation of calcium as $CaSO_4$. The magnesium extraction remains relatively constant even if it was conducted at high leaching temperatures.

The XRD results revealed that goethite peaks are significantly disappeared with an increase of the leaching temperature, which means that the iron-bearing minerals have been taken into the leach solution. The intensity of the quartz peaks signicantly increased with increasing the leaching temperature (see supplementary Fig. S-4). The quartz and hematite peaks became dominant peaks in the residue when the experiments were performed at 90°C and 5 M H_2SO_4 concentration. Since the selective extraction of manganese was targeted during the leaching process, it was necessary to determine the parameters where the manganese extraction was high but the iron extraction was low. These experimental conditions were determined to be 1 M H_2SO_4 concentration, 1 h leaching time, 300 rpm stirring speed, 70°C leaching temperature, at which 2.16% Fe and 11.54% Mn extractions were achieved under the conditions explored. By keeping these values constant, the use of biomass as reductant was investigated in further leaching tests.

Leaching Experiments with Reductant (Waste Biomass)

Initially, to determine organic acids in the waste biomass, the HPLC analysis was performed (see supplementary Fig. S-5). The analysis demonstrated that the liquor contains 4234.148 ± 222.24 mg/L oxalic acid, 1754.524 ± 48.661 mg/L citric acid, 10,225.14 ± 169.64 mg/L malic acid, 1498.002 ± 80.652 mg/L acetic acid, and trace amounts of succinic, fumaric, and butyric acids, which are possible reducing organic agents during the reductive leaching process. The possible reactions for manganese extraction using these acids are shown in Eq. 10.

$$3MnO_2 + C_2H_2O_2 + 6H^{(+a)} = 3Mn^{(+2a)} + 2CO_2(g) + 4H_2O(I) \quad (4)$$

$$9MnO_2 + C_6H_8O_7 + 18H^{(+a)} = 9Mn^{(+2a)} + 6CO_2(g) + 13H_2O(I) \quad (5)$$

$$6MnO_2 + C_4H_6O_5 + 12H^{(+a)} = 6Mn^{(+2a)} + 4CO_2(g) + 9H_2O(I) \quad (6)$$

$$4MnO_2 + C_2H_4O_2 + 8H^{(+a)} = 4Mn^{(+2a)} + 2CO_2(g) + 6H_2O(I) \quad (7)$$

$$7MnO_2 + C_4H_6O_4 + 14H^{(+a)} = 7Mn^{(+2a)} + 4CO_2(g) + 10H_2O(I) \quad (8)$$

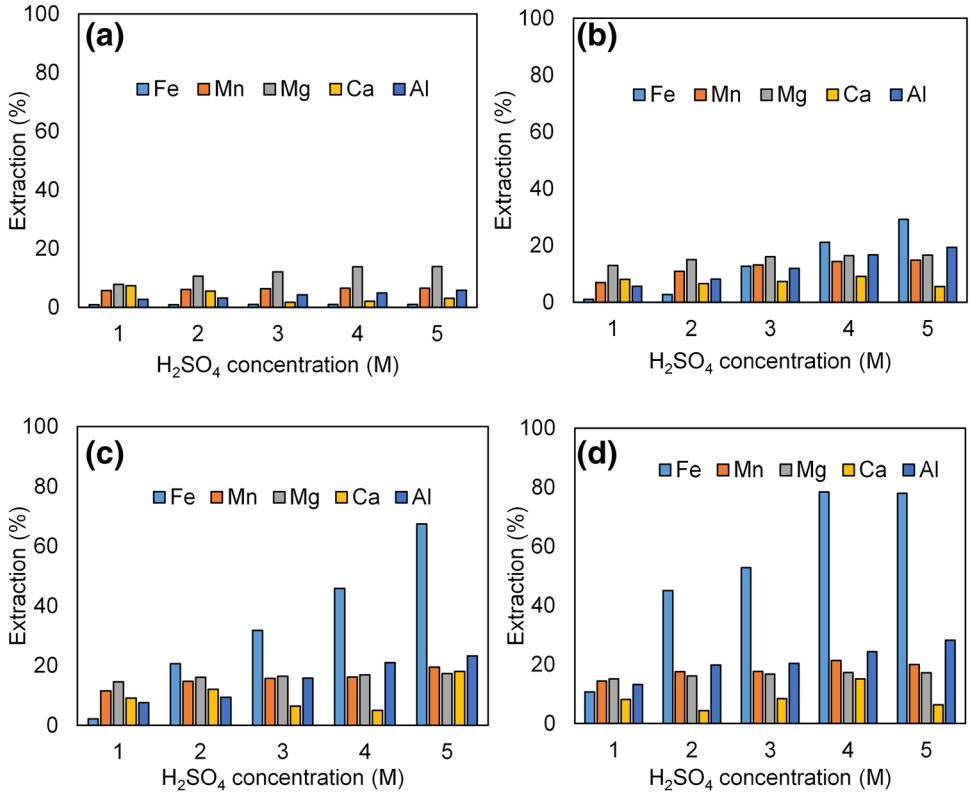

Fig. 2. Dissolutions in the experiments conducted at 300 rpm, 100 g/L ore sample, 1 h leaching time, and varying H_2SO_4 concentrations at 25°C (a), 50°C (b), 70°C (c), and 90°C (d) temperatures.

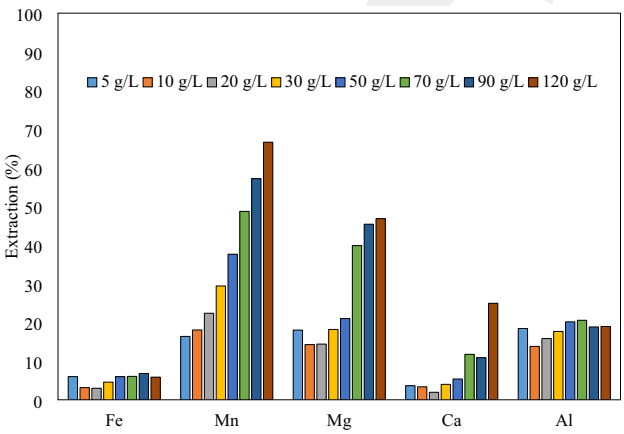

Fig. 3. Dissolutions in the tests conducted at 300 rpm, 100 g/L ore sample, 1 h, 1 M H_2SO_4, and varying horse dung additions at 70 °C.

$$6MnO_2 + C_4H_4O_4 + 12H^{(+a)} = 6Mn^{(+2a)} + 4CO_2(g) + 8H_2O(I) \quad (9)$$

$$10MnO_2 + C_4H_8O_2 + 20H^{(+a)} = 10Mn^{(+2a)} + 4CO_2g + 14H_2O(I) \quad (10)$$

The reductive leaching experiments were carried out using biomass as a reducing agent in 1 M H_2SO_4 solution at 70°C for 1 h (Fig. 3). It was observed that the extraction percentages of the metals slightly increased with increasing biomass addition. The highest manganese extraction, 66.62%, was achieved when 120 g/L of reductant was used. At this reductant concentration, the extraction of iron reached the value of 5.86%. The highest magnesium extractions were found to be 45.41% and 46.84% when using 90 g/L and 120 g/L biomass, respectively.

When the XRD patterns of the residue are examined, the manganite and ramsdellite peaks have decreased or disappeared, which confirms the manganese extraction (see supplementary Fig. S-6). In these experiments, although the peaks of the manganese minerals disappeared, the quartz peak intensities remained almost constant or slightly decreased. This is attributed to the reductant not being fully dissolved in the lixiviant causing an increase in the amount of leach residue. Also, the gypsum peaks confirm the precipitation of calcium as $CaSO_4$.

Development of the Reductive Leaching Experiment and Kinetic Study

The reductive leaching experiments were carried out at 25°C, 50°C, 70°C, and 90°C temperatures and four different durations under the following conditions: 300 rpm stirring speed, 1 M H_2SO_4 concentration, 100 g/L solid ratio, and 120 g/L biomass

reductant. Especially in the experiments carried out at 90°C, the manganese extraction values were very high. At this temperature, the manganese extraction was almost completely achieved within 2 h (Fig. 4d).

The manganese dissolution mechanism using biomass was investigated, which has not previously been applied as reductant for manganiferous iron ores. After obtaining dissolution values at different temperatures and durations, it was investigated to what degree manganese dissolution rates are suitable for kinetic reaction patterns. When the reaction degree was determined, an Arrhenius plot was constructed by using rate constants. The Arrhenius formula is shown in Eq. (11):

$$k = Ae^{\frac{-Ea}{RT}} \tag{11}$$

where k is the rate constant (min^{-1}), T the absolute temperature (K), A pre-exponential factor, E_a the activation energy of the reaction (kJ/mol), and R a universal constant (8.314 J mol^{-1} K^{-1}).

Since the slope of the line in the Arrhenius plot constructed with the help of rate constants is equal to $-E_a/R$, the activation energies of the reactions are calculated with the help of the equation with one unknown. In the light of the manganese dissolution values, it was determined that the reactions followed first-order reaction kinetics (see supplementary Fig. S-7a). The Arrhenius plot was created with the help of rate constants (see supplementary Fig. S-7b), and the activation energy was found to be 38.64 kJ/mol. The manganese dissolution reaction under these experimental conditions is chemically controlled which is consistent with the finding of Robertson et al..[51] They reported that reactions with an activation energy greater than 25 kJ/mol are chemically controlled. The reductive leaching process revealed that 99.80% of Mn along with 17.76% of Fe were extracted into the leach solution under the determined conditions: 1 M H_2SO_4 concentration, 120 g/L biomass, 1/10 solid to liquid ratio, 300 rpm stirring speed, 90°C leaching temperature, and 3 h leaching time. The subsequent precipitation and carbothermal reduction tests were carried out using the pregnant leach solution and residue obtained under the determined leaching conditions.

Carbothermal Reduction Study

In the carbothermal reduction process, insoluble biomass in the reductive leaching process acts as a carbon provider. The CO and CO_2 gases resulting from combustion reduce the iron minerals such as hematite and goethite. The removal of oxygen by reduction leads to the conversion of iron content to magnetite minerals. The possible reactions occurring in the carbothermal reduction process are given in Eqs. 12–15. Samohuos et al.[52] and Peng et al.[53] indicated that iron conversion develops as $Fe_2O_3 > Fe_3O_4 > FeO > Fe$ in the carbothermal reduction process when the process temperature increases. It was seen that all of the iron content is converted into magnetite mineral in the reduction process at temperatures of 600°C and 700°C (see supplementary Fig. S-8). The XRD pattern of the

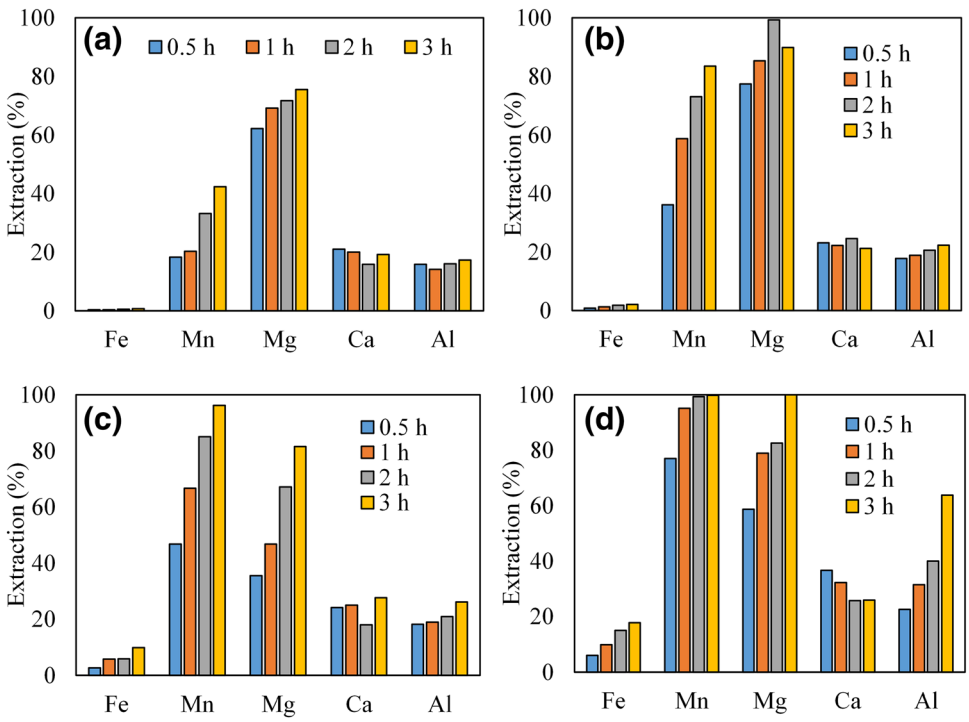

Fig. 4. Dissolution rates of the contents as a function of leaching times performed at 25°C (a), 50°C (b), 70°C (c), and 90°C (d) using 120 g/L biomass reductant.

sample belonging to the reduction process at 700°C was examined. It was found that the intensity of the magnetite peaks is higher than that at 600°C, which means that a better crystallization (magnetite conversion) was achieved. At 800°C, the iron content started to form a compound with silicates and fayalite minerals, which is a paramagnetic property and not possible to be recovered by the magnetic separation technique. The fayalite mineral is also seen as a dominant peak at 900°C. In addition, metallic iron peaks (Fe nugget at 45°, 65°, and 82° peaks) were observed with a high reduction of iron contents at high temperatures.

$$C + O_2 \rightarrow CO_2 \quad (12)$$

$$CO_2 + C \rightarrow 2CO \quad (13)$$

$$2C + O_2 \rightarrow 2CO \quad (14)$$

$$3Fe_2O_3 + CO \rightarrow 2Fe_3O_4 + CO_2 \quad (15)$$

Magnetic susceptibility (S) was calculated by using Eq. (16). As a result of the XRD analysis, the magnetic hysteresis (M–H) curves of the sample reduced in 10 min at 700°C, and the sample before the reduction was created for 0–3 T magnetic field intensity by a physical property measurement system (DynaCool-9) equipped with the vibrating sample magnetometer option (Fig. 5). The increase in the magnetic properties of the sample are visible through the reduction process. XRF analysis revealed that the reduced sample consists of 50.92% Fe_2O_3, 30.46%SiO_2, 12.21%SO_3, 5.46% CaO. and 0.95 % MnO.

$$S = \frac{M}{H} \quad (16)$$

where S is the magnetic susceptibility (g.Coulomb/amp), M the magnetization intensity (g.Coulomb/m), and H the magnetic field intensity (amp/m)

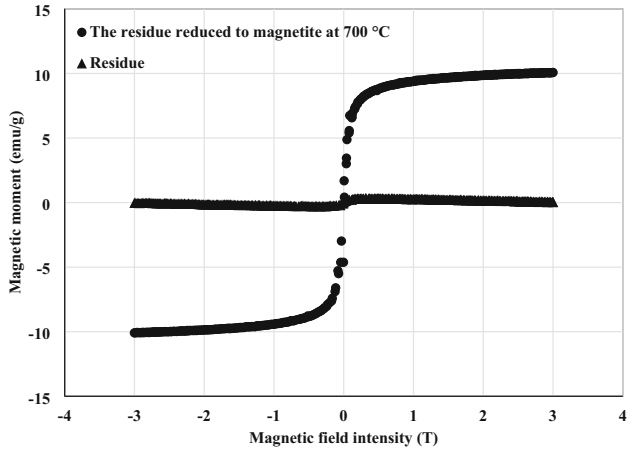

Fig. 5. M–H curves of the residue and the converted sample.

The First Step Precipitation Study

The content of the PLS produced under the above leaching conditions is given in Table S-I. The pH of the PLS was determined to be 0.53. The pH value of the solution was initially increased up to 5 with 5M NaOH solution addition. The main reason for the first step of precipitation is the removal of impurities such as Fe and Al.

Pakarinen and Paatero[54] reported that Fe^{2+} has a poor ability to precipitate as hydroxide, and is generally oxidized into Fe^{3+} in industrial processes and then precipitated in the form of hydroxide. Fe^{3+} precipitates in hydroxide form around pH 4–5. Higher pH values are required for the precipitation of Fe^{2+} ions. Manganese begins to precipitate from pH 7 and, therefore, the amount of Fe^{2+} ions play an active role in the selective separation of manganese and iron. Krauskopf[55] reported that, unless the Mn/Fe ratio is too high, iron is primarily precipitated for manganese recovery in inorganic processes.

The precipitation reaction can be written according to Eq. (17). Figure S-9 shows the equilibrium constants (log K) for the precipitation of iron, manganese, magnesium, and calcium as a function of temperature over the range 0–100°C, which is useful for the recovery of metal hydroxides. It is seen that, at 25°C, the values of log K follow the descending order: $Fe(OH)_3 > Al(OH)_3 > Fe(OH)_2 > Mn(OH)_2 > Mg(OH)_2 > Ca(OH)_2$. The low value of log K for $Ca(OH)_2$ in Fig. S-9 indicates the need for a high pH to precipitate $Ca(OH)_2$.

$$Mn^{n+} + nH_2O = M(OH)_n + nH^+(\text{form} = 2,3; M = Fe, Al, Mn, Mg, Ca) \quad (17)$$

The iron and aluminum precipitated with increasing solution pH (see supplementary Fig. S-10). The manganese, calcium, and magnesium remained in the solution almost completely. 80% Fe was precipitated at 25°C temperature and pH around 4–5. Similar results were observed for the aluminum precipitation. It was seen that the precipitation percentage of aluminum ($Al(OH)_3$, log K: − 11.318 at 25°C) is interestingly higher than iron ($Fe(OH)_3$, log K: − 4.034 at 25°C). This might be due to the presence of organic agents that can make more stable complexes with iron than the aluminum and sulfate ion concentration in the solution. It was observed that the iron and aluminum were almost completely precipitated at 60°C and pH 5. The optimum precipitation conditions in the first step were determined to be pH 5, 350 rpm stirring speed, and 60°C precipitation temperature. The precipitation test results are compatible with those of previous studies in the literature.[54,56,57] Therefore, the remaining solution under these optimum conditions was collected for the use of the second step precipitation tests.

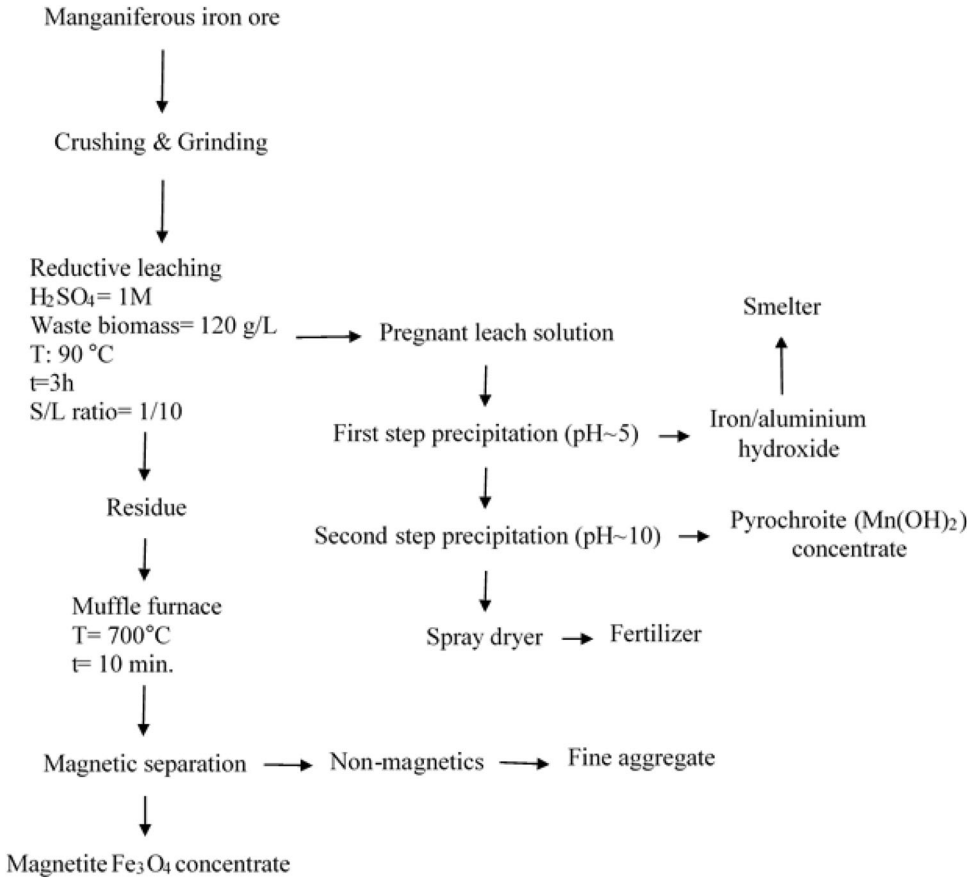

Fig. 6. Proposed flowsheet for the separation of manganese and iron from the manganiferous iron ore.

The Second Step Precipitation Study

The content of the solution used in the second step is given in Table S-II. The pH of the solution was 5.16. The second step precipitation experiments were carried out at 25°C by adjusting the solution pH. Figure S-11 shows the chemical equilibrium diagrams for the second step precipitation. The metal ion concentrations (216.43 mM Mn, 29.87 mM Mg, and 1 mM Ca) were used to draw the diagrams using Medusa software. As can be seen from the equilibrium diagram, the manganese begins to precipitate above pH 7.5. The manganese is completely precipitated at pH 10. The magnesium starts to precipitate above pH 9. Calcium, on the other hand, has a much higher precipitation pH. Monhemius[58] reported that high pH values (> 12) are required for the precipitation of calcium. The manganese was almost completely precipitated around pH 10 (see supplementary Fig. S-12), which is consistent with the finding of Zhang and Cheng.[56] They reported that manganese precipitation begins at pH around 7 until 11 and magnesium starts to precipitate after pH 9. The obtained precipitation test results are consistent with the Medusa HSC chemistry software, and the findings of previous researchers.

The XRD analysis of the precipitates is given in Fig. S-13. The precipitate was identified as pyrochroite $Mn(OH)_2$ mineral, which confirms the precipitation test results. The widespread XRD peaks (halo peaks) indicate that the precipitates are mostly amorphous structures. As a result of the second step precipitation tests, the selective precipitation of manganese can be achieved at pH 10. Based on the experimental results obtained from the bench-scale study, a flowsheet was proposed for the separation of manganese and iron from the manganiferous iron ore (Fig. 6).

CONCLUSION

Depletion of primary ore resources and the effect of technological developments necessitate the beneficiation of complex ores that were not preferred before. Sustainable development requires good waste management as well as obtaining the maximum benefit from natural resources. In this study, the separation of manganese and iron from a manganiferous iron ore via reductive acid leaching followed by precipitation and carbothermal reduction processes was investigated. Waste biomass was used as a reducing agent in both the reductive leaching and carbothermal reduction processes. The biomass was only added in the reductive leaching

step and the undissolved biomass particles in the leach residue played a carbon-providing role in magnetite conversion. Under the determined leaching conditions, 99.80% Mn and 17.76% Fe were taken into the leach solution, while 98.58% Mn was selectively precipitated from the pregnant leach solution as $Mn(OH)_2$ in the second step precipitation. The leach residue obtained from the predetermined leaching conditions was ignited at 700°C for 10 min. to convert the entire iron content into magnetite mineral, which can be easily recovered by magnetic separation. Based on the experimental results, the proposed flowsheet can be used for the separation of manganese and iron from manganiferous iron ores.

ACKNOWLEDGEMENTS

This research was financially supported by The Scientific and Technological Research Council of Turkey (TÜBİTAK Project Code: 119M690) and Cukurova University (FBA-202-13057). The authors also thank Dr. Ekin Köken for preliminary carbothermal reduction tests.

FUNDING

Türkiye Bilimsel ve Teknolojik Araştirma Kurumu, 119M690 and Çukurova Üniversitesi, FBA-2020-13057.

CONFLICT OF INTEREST

The authors declare that they have no conflict of interest.

SUPPLEMENTARY INFORMATION

The online version contains supplementary material available at https://doi.org/10.1007/s11837-021-05057-3.

REFERENCES

1. V. Kuleshov, *Isotope Geochemistry: The Origin and Formation of Manganese Rocks and Ores* (Elsevier, Amsterdam, 2016), p 440.
2. T. Coetsee, *Miner. Process. Extract. Metall. Rev.* 39(5), 351 (2018).
3. B. Liu, Y. Zhang, M. Lu, Z. Su, G. Li, and T. Jiang, *Miner. Eng.* 131, 286. (2019).
4. IBOM. https://ibm.gov.in/writereaddata/files/11052014103838Manganese_Ore_Vision_2020_and_Beyond.pdf. Accessed 20 January 2020.
5. H, Hartmann. Spiegeleisen manufacturing. in Fifth Annual Report of the Geological Survey of Indiana. 71 (1874).
6. H, Vapur, and S. Top, *J. Fac. Eng. Archit.* 31(1), 293 (2016).
7. S.S. Rath, S.K. Tripathy, D.S. Rao, and K. Biswal, *Trans. Indian Inst. Met.* 71(4), 861 (2018).
8. A. Mehdilo, M. Irannajad, and M.R. Hojjati-Rad, *Physicochem. Probl. Miner. Process.* 49(2), 725 (2013).
9. P. Mishra, B. Mohapatra, and K. Mahanta, *J. Miner. Mater. Charact. Eng.* 8(01), 47 (2009).
10. K. Shrimali, V. Atluri, Y. Wang, S. Bacchuwar, X. Wang, and J.D. Miller, *J. Colloid Interf. Sci.* 524, 337 (2018).
11. H. Vapur, S. Top, M. Altiner, S. Uçkun, and M. Sarikaya, *Particul. Sci. Technol.* 38(4), 409. (2020).
12. J. Yu, Y. Han, Y. Li, and P. Gao, *Int. J. Miner. Process.* 168, 102. (2009).
13. V. Singh, T.K. Ghosh, Y. Ramamurthy, and V. Tathavakar, *Int. J. Miner. Process.* 99(1–4), 84. (2011).
14. S.K. Tripathy, P.K. Banerjee, and N. Suresh, *Int. J. Miner. Metall. Mater.* 22(7), 661. (2015).
15. D. Fan and P. Yang, *Ore Geol. Rev.* 15(1–3), 1. (1999).
16. A.W. Rose, B. Means, and P. Shah. Methods for passive removal of manganese from acid mine drainage. https://citeseerx.ist.psu.edu/viewdoc/download?doi=10.1.1.501.9735&rep=rep1&type=pdf. Accessed 20 January 2020.
17. J. Gutzmer and N.J. Beukes. Geology—Vol. IV—Iron and manganese ore deposits: mineralogy, geochemistry, and economic geology. http://www.eolss.net/sample-chapters/c01/e6-15-06-03.pdf. Accessed 19 January 2020.
18. K. Li, G. Chen, X. Li, K. Peng, R. Ruan, M. Omran, and J. Chen, *Biores. Technol.* 294, 122217. (2019).
19. K. Li, J. Chen, X. Li, K. Peng, C. Srinivasakannan, and G. Chen, *Powder Technol.* 360, 846. (2020).
20. Y. Gao, M. Olivas-Martinez, H.Y. Sohn, H.G. Kim, and C.W. Kim, *Metall. Maters. Trans. B* 43(6), 1465. (2012).
21. Z. You, G. Li, Y. Zhang, Z. Peng, and T. Jiang, *Hydrometallurgy* 156, 225. (2015).
22. F. Veglio and L. Toro, *Hydrometallurgy* 36(2), 215. (1994).
23. T.A. Lasheen, M.N. El-Hazek, A.S. Helal, and W. El-Nagar, *Int. J. Miner. Process.* 92(3–4), 109. (2009).
24. G. Furlani, E. Moscardoni, F. Pagnanelli, F. Feralla, F. Veglio, and L. Toro, *Hydrometallurgy* 99(1–2), 115. (2009).
25. N. Muthalib, N. Abdullah, and S. Ismail, *ASEAN Eng. J.* 8(2), 64. (2018).
26. B. Nayak, K. Mishra, and R. Paramguru, *J. Appl. Electrochem.* 29(2), 191. (1999).
27. F. Momade, and Z.G. Momade, *Hydrometallurgy* 51(1), 103. (1999).
28. P.K. Naik, L. Sukla, and S. Das, *Hydrometallurgy* 54(2–3), 217. (2000).
29. R. Sahoo, P. Naik, and S. Das, *Hydrometallurgy* 62(3), 157. (2001).
30. D. Hariprasad, B. Dash, M.K. Ghosh, and S. Anand, *Miner. Eng.* 20(14), 1293. (2007).
31. Z. Cheng, G. Zhu, and Y. Zhao, *Hydrometallurgy* 96(1–2), 176. (2009).
32. X. Tian, X. Wen, C. Yang, Y. Liang, Z. Pi, and Y. Wang, *Hydrometallurgy* 100(3–4), 157. (2010).
33. T. Qing, H. Zhong, S. Wang, J. Li, and G. Liu, *Trans. Nonferr. Metal. Soc. China* 24(3), 861. (2014).
34. S. Xiong, X. Li, P. Liu, S. Hao, F. Hao, Z. Yin, and J. Liu, *Miner. Eng.* 125, 126. (2018).
35. B. Ghafarizadeh, F. Rashchi, and E. Vahidi, *Miner. Eng.* 24(2), 174. (2011).
36. A. Nayl, I. Ismail, and H. Aly, *Int. J. Miner. Process.* 100(3–4), 116. (2011).
37. Y. Lu, H. Ma, R. Huang, A. Yuan, Z. Huang, and Z. Zhaou, *Metall. Mater. Trans. B* 46(4), 1709. (2015).
38. C. Li, H. Zhong, S. Wang, J. Xue, F. Wu, and Z. Zhang, *Trans. Nonferr. Metal. Soc. China* 25(5), 1677. (2015).
39. E. Prasetyo, E. Purwaningsih, and W. Astuti, *Mining Metall. Explor.* 36(5), 1003. (2019).
40. M.K. Sinha, W. Purcell, and W.A. Van Der Westhuizen, *Miner. Eng.* 154, 106406. (2020).
41. K. Li, Q. Jiang, G. Chen, L. Gao, J. Peng, Q. Chen, S. Koppala, and M. Omran, *J. Chen. Biores. Technol.* 319, 124172. (2021).
42. F. Wu, H. Zhong, S. Wang, S. Lai, and J. Cent, *South Univ.* 21, 1763. (2014).
43. X. Lu, J. Wang, H.M. Al-Qadiri, C.F. Ross, J.R. Powers, J. Tang, and B.A. Rasco, *Food Chem.* 129(2), 637. (2011).
44. S.D. Silva, R.P. Feliciano, L.V. Boas, and M.R. Bronze, *Food Chem.* 150, 489. (2014).

45. R.K. Singh, A. Kukrety, O.P. Sharma, S. Baranwal, N. Atray, and S.S. Ray, *J. Indust. Eng. Chem.* 37, 27. (2016).
46. P. Guerrero, T. Garrido, I. Leceta, and K. De La Caba, *Euro. Polym. J.* 49(11), 3713. (2013).
47. P. Demir, S. Onde, and F. Severcan, *Spectrochim. Acta Part A* 135, 757. (2015).
48. P. Guerrero, J.P. Kerry, and K. De La Caba, *Carbohydr. Polym.* 111, 598. (2014).
49. M. Grube, J.G. Lin, P.H. Lee, and S. Kokovicha, *Geoderma* 130(3–4), 324. (2006).
50. A.S. Baharuddin, N.A.A. Rahman, U.K. Shan, M.A. Hassan, M. Wakika, and Y. Shirai, *Afr. J. Biotechnol.* 10(41), 8082. (2011).
51. S. Robertson, M. Jeffrey, H. Zhang, and E. Ro, *Metall. Mater. Trans. B* 36(3), 313. (2005).
52. M. Samouhos, M. Taxiarchou, P.E. Tsakiridis, and K. Potiriadis, *J. Hazard. Mater.* 254, 193. (2013).
53. T. Peng, L. Xu, and L. Luo, *Open Chem.* 15(1), 389. (2017).
54. J. Pakarinen and E. Paatero, *Miner. Eng.* 24(13), 1421. (2011).
55. K.B. Krauskopf, Separation of manganese from iron in the formation of manganese deposits in volcanic associations. in Symp. Del. Mangenso. 20th. Int. Geol. Cong., Mexico, 119–131 (1957).
56. W. Zhang and C.Y. Cheng, *Hydrometallurgy* 89(3–4), 160. (2007).
57. D.C. Ong, M.D.G. De Luna, S.M.B. Pingul-Ong, and C.C. Kan, *J. Environ. Manag.* 223, 723. (2018).
58. A.J. Monhemius, *Trans. Inst. Min. Metall. Sect. C* 86, 202. (1977).